Electronic Supplementary Material (ESI) for Chemical Communications

One-dimensional Confinement of Nanosized Metal Organic Framework in Carbon Nanofibers for Improved Gas Adsorption

Pradip Pachfule‡, Beena K. Balan‡, Sreekumar Kurungot* and Rahul Banerjee*

[a] *Physical/Materials Chemistry Division, National Chemical Laboratory, Dr. Homi Bhabha Road, Pune-411008, India.*

E-mail: k.sreekumar@ncl.res.in Fax: + 91-20-25902636; Tel: + 91-20-25902566

E-mail: r.banerjee@ncl.res.in Fax: + 91-20-25902636; Tel: + 91-20-25902535

Supporting Information

Content

Section 1. Detailed synthesis procedures MOF hybrids:

1, 4-Benzene dicarboxylic acid (Terephthalic acid), *N*, *N*-Diethylformamide (DEF) and $Zn(NO_3)_2.6H_2O$ were purchased from Aldrich Chemicals. All starting materials were used without further purification. All experimental operations were performed in air and all the stock solutions were prepared in *N*, *N*-Diethylformamide (DEF).

Synthesis of MOF@PCNF: $Zn(NO_3)_2.6H_2O$ (0.1 gm) and terephthalic acid (1, 4-benzene dicarboxylic acid) (0.4 gm) were dissolved in 10 ml N, N-Diethylformamide (DEF) and mixed well by ultra-sonication (5 min) to get a clear solution in a glass vial. To this solution a weighed amount of the PCNF (45 mg) was added. To facilitate the entry of the precursor solution in the inner cavity of the CNFs, this was subjected to extensive sonication using a probe type sonicator (10 sec pulse for 5 times). This slurry was then kept at 90 °C for 48 hours for the complete formation of MOF crystals. The resulting hybrid material was purified and separated from the unattached MOFs by repeated centrifugation (5 times) at 2000 rpm in the same solvent used for the synthesis. As there is an accountable difference in the density of pure MOFs and the hybrid material, during centrifugation pure MOFs were settled down at the bottom and could be separated from the hybrid material easily. The resulting hybrid material MOF@PCNF was collected and dried in atmospheric conditions.

Synthesis of MOF@FCNF: $Zn(NO_3)_2.6H_2O$ (0.1 gm) and terephthalic acid (1, 4-benzene dicarboxylic acid) (0.4 gm) in were dissolved in 10 ml N, N-Diethylformamide (DEF) and mixed well by ultra-sonication (5 min) to get a clear solution in a glass vial. To this solution a weighed amount of the FCNF (45 mg) was added. In this case, pristine CNFs (PCNF) activated by an H_2O_2 treatment at 60 °C for 6 hours to introduce functional groups (FCNF) was used. The same

synthesis approach was performed to load MOF on FCNF and to get the phase pure MOF@FCNF.

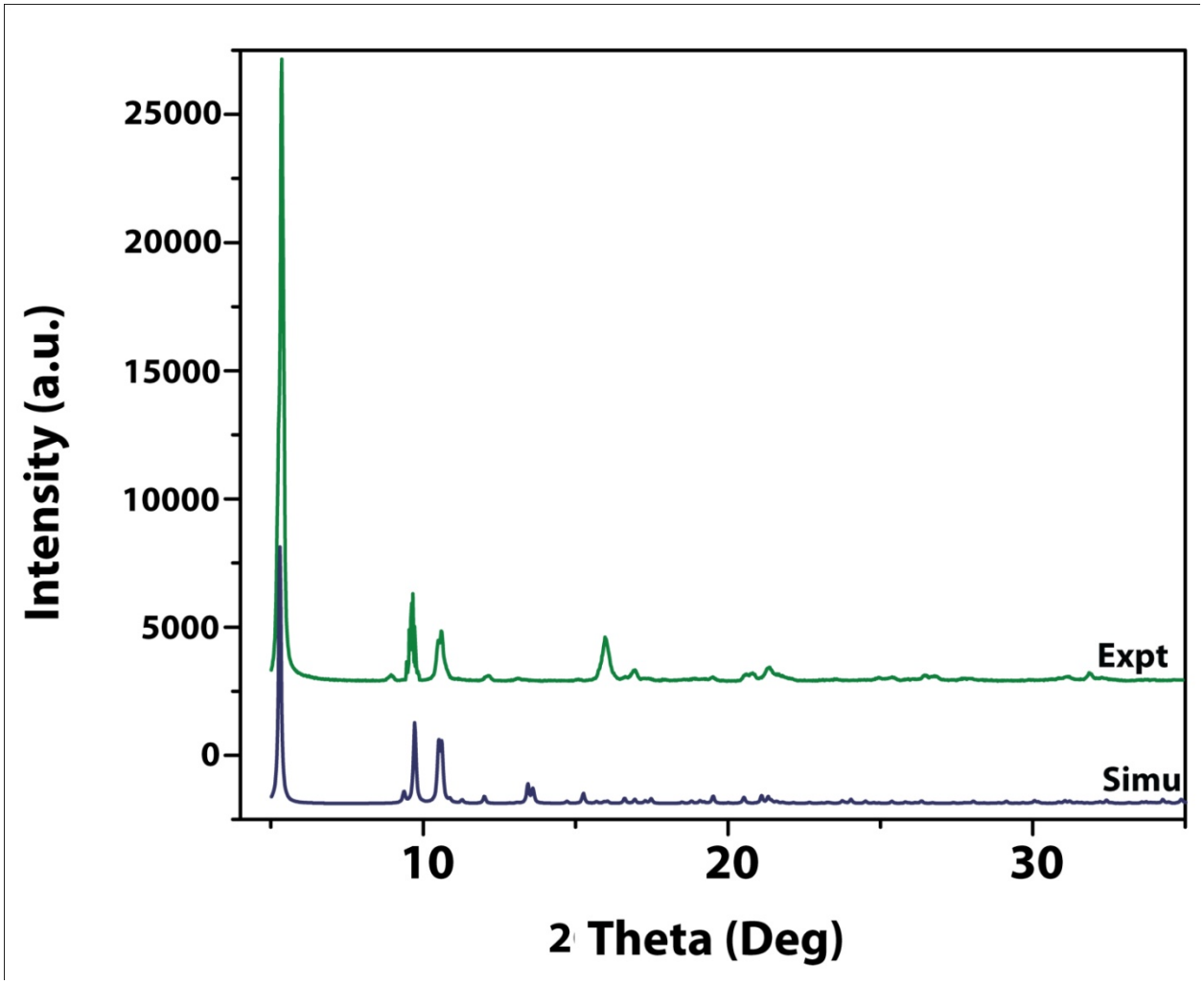

Figure S1. *Comparison of the experimental PXRD pattern of as-synthesized MOF-2 (top) with the simulated from single crystal structure of MOF-2 (bottom).*

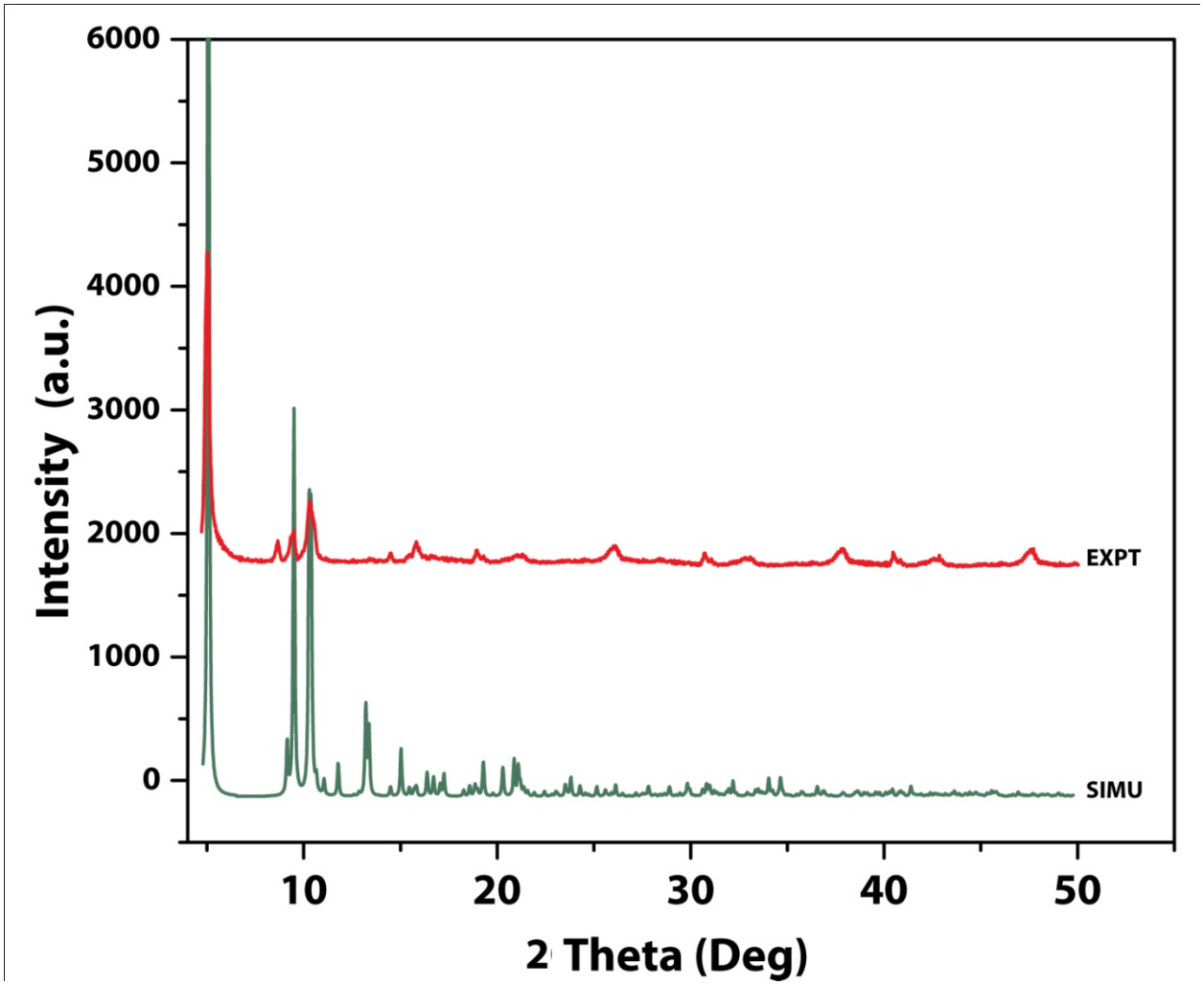

Figure S2. *Comparison of the experimental PXRD pattern of as-synthesized MOF@FCNF (top) with the simulated from single crystal structure of MOF-2 (bottom).*

Section 2: Scanning Electron Microscopy (SEM) Images:

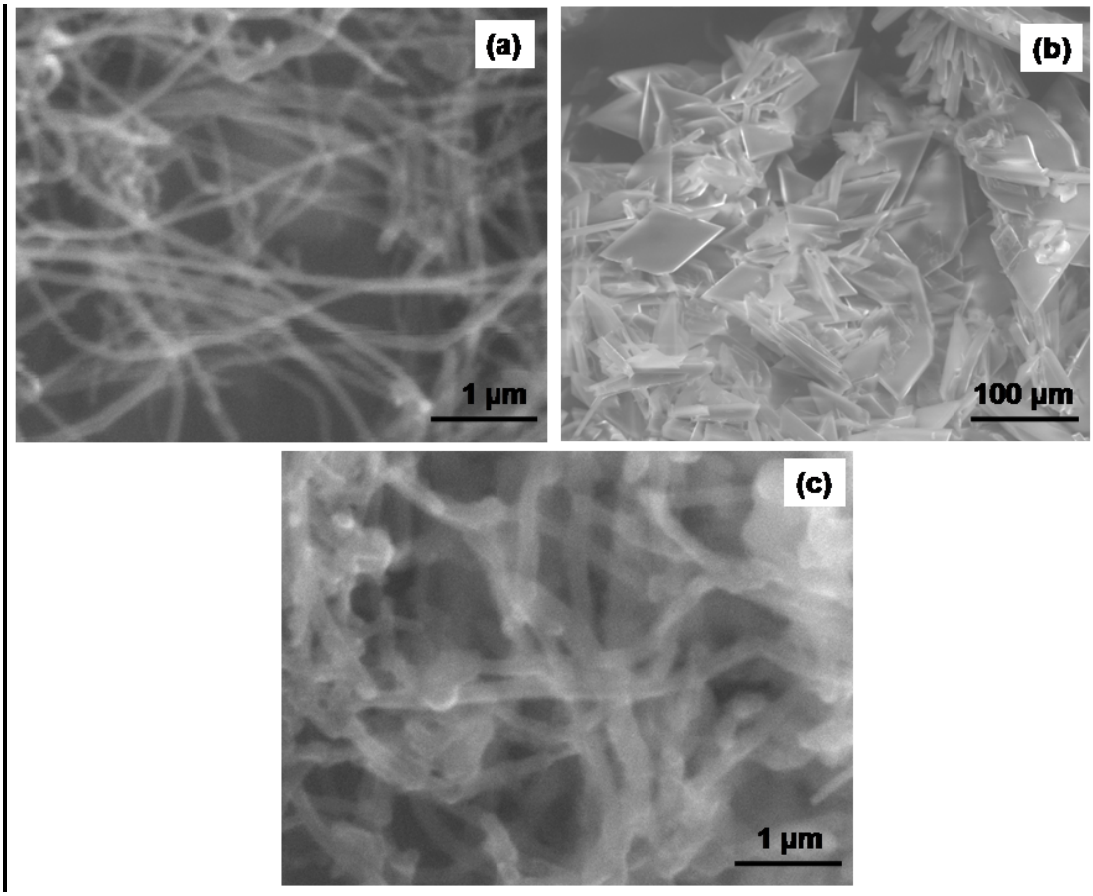

Figure S3. *Comparison of the SEM images of (a) pristine CNF, (b) pure MOF-2 and (c) MOF@FCNF.*

The SEM images of the pristine carbon nanofibers given in Figure S1 (a) clearly depict that the length of these nanofibers is in few micrometers and diameter is ca. 100 ± 20 nm. Figure (b), which is the SEM images of pure MOF-2 indicates that the size of the MOF is in micrometers, typically in the range of 100 µm. It is also clear from the image that the growth of MOFs is not uniform and there is polydispersity in size as well as in shape. The SEM image of MOF@FCNF given in Figure S1(c) demonstrate a clear enhancement in the diameter of the CNFs after the MOF incorporation. The observed diameter is ca. 150 ± 20 nm and this enhancement in the diameter gives an indication for the incorporation of the MOF in CNFs. However, the presence

of MOF in and out of CNF cannot be detected from the SEM images due to its nanosize, which will be explained in the latter sections. But it should be noted that micro-sized MOF are not attached to the CNFs. From the SEM images of the hybrid material it can also be confirmed that the unattached MOFs are not present in the sample, which implies the effectiveness of the washing strategy we adopted for the purification and separation of the material from the unattached MOFs.

Section 3: Single crystal X-ray diffraction data collection, structure solution and refinement procedures for MOF-2:

The crystal structure of Zn-terephthalate MOF (MOF-2) has been reported previously by Stock and co-workers (Ref. Code: VEGMOK04, CCDC No. 281855, E. Biemmi, T. Bein and N. Stock, Solid State Sciences, 2006, ***8****, 363–370). To confirm the MOF formed in the reaction vessel along with MOF@FCNF hybrid, we have collected the microcrystal's of MOF-2 from the vial (refer figure S3 (b) for morphology of the MOF-2 crystals) by centrifugation at 2000 rpm in the same solvent used for the synthesis. Although the crystal structure of MOF-2 has been reported previously, in order to confirm the formation of the exact phase of the Zn-terephthalate MOF, we have collected the Single Crystal data for this crystals. The strategies for general data collection, experimental and refinement details for MOF-2, crystal data and structure refinement for MOF-2 and ORTEP diagram has been discussed below:*

General Data Collection and Refinement Procedures:

Single crystal data were collected on Bruker SMART APEX three circle diffractometer equipped with a CCD area detector and operated at 1500 W power (50 kV, 30 mA) to generate Mo K_α radiation (λ=0.71073 Å). The incident X-ray beam was focused and monochromated using Bruker Excalibur Gobel mirror optics. Crystal of MOF-2 reported in the paper was mounted on nylon CryoLoop (Hampton Research) with Paraton-N (Hampton Research).

Initial scans of this specimen were performed to obtain preliminary unit cell parameters and to assess the mosaicity (breadth of spots between frames) of the crystal to select the required frame width for data collection. In every case frame widths of 0.5° were judged to be appropriate

and full hemispheres of data were collected using the *Bruker SMART*[1] software suite. Following data collection, reflections were sampled from all regions of the Ewald sphere to re-determine unit cell parameters for data integration and to check for rotational twinning using *CELL_NOW*[2]. In no data collection was evidence for crystal decay encountered. Following exhaustive review of the collected frames the resolution of the dataset was judged. Data was integrated using Bruker *SAINT*[3] software with a narrow frame algorithm and a 0.400 fractional lower limit of average intensity. Data was subsequently corrected for absorption by the program *SADABS*[4]. The space group determination and test for merohedral twinning were carried out using *XPREP*[3]. In this case, the highest possible space group was chosen.

Structure was solved by direct methods and refined using the *SHELXTL 97*[5] software suite. Atoms were located from iterative examination of difference F-maps following least squares refinements of the earlier models. Final model was refined anisotropically (if the number of data permitted) until full convergence was achieved. Hydrogen atoms were placed in calculated positions (C-H = 0.93 Å) and included as riding atoms with isotropic displacement parameters 1.2-1.5 times U_{eq} of the attached C atoms. In some cases modeling of electron density within the voids of the frameworks did not lead to identification of recognizable solvent molecules in these structures, probably due to the highly disordered contents of the large pores in the frameworks. Highly porous crystals that contain solvent-filled pores often yield raw data where observed strong (high intensity) scattering becomes limited to ~1.0 Å at best, with higher resolution data present at low intensity. A common strategy for improving X-ray data, increasing the exposure time of the crystal to X-rays, did not improve the quality of the high angle data in these cases, as the intensity from low angle data saturated the detector and minimal improvement in the high angle data was achieved. Additionally, diffuse scattering from the highly disordered

solvent within the void spaces of the framework and from the capillary to mount the crystal contributes to the background and the 'washing out' of the weaker data. The only optimal crystals suitable for analysis were generally small and weakly diffracting. Unfortunately, larger crystals, which would usually improve the quality of the data, presented a lowered degree of crystallinity and attempts to optimize the crystal growing conditions for large high-quality specimens have not yet been fruitful. Single Crystal X-ray Diffraction data for MOF-2 was collected at 298(2) K. Electron density within void spaces has not been assigned to any guest entity but has been modeled as isolated oxygen and/or carbon atoms. The foremost errors in all the models are thought to lie in the assignment of guest electron density. Structures were examined using the *ADDSYM* subroutine of *PLATON*[7] to assure that no additional symmetry could be applied to the models. Ellipsoids in *ORTEP* diagrams are displayed at the 50% probability level unless noted otherwise. For this structure we noted that elevated R-values are commonly encountered in MOF crystallography for the reasons expressed above by some research groups.[8-17] Table S1 contains crystallographic data for the MOF-2.

1. Bruker (2005). *APEX2*. Version 5.053. Bruker AXS Inc., Madison, Wisconsin, USA.
2. Sheldrick, G. M. (2004). *CELL_NOW*. University of Göttingen, Germany. Steiner, Th. (1998). *Acta Cryst*. B54, 456–463.
3. Bruker (2004). *SAINT-Plus* (Version 7.03). Bruker AXS Inc., Madison, Wisconsin, USA.
4. Sheldrick, G. M. (2002). *SADABS* (Version 2.03) and *TWINABS* (Version 1.02).University of Göttingen, Germany.
5. Sheldrick, G. M. (1997). *SHELXS '97* and *SHELXL '97*. University of Göttingen, Germany.
6. WINGX

7. A. L. Spek (2005) PLATON, *A Multipurpose Crystallographic Tool*, Utrecht University, Utrecht, The Netherlands.
8. Dakin, L. A., Ong P. C., Panek, J. S., Staples, R. J. & Stavropoulos, P. *Organometallics* **19**, 2896-2908 (2000).
9. Noro, S., Kitaura, R., Kondo, M., Kitagawa, S., Ishii, T., Matsuzaka, H. & Yamashita, M. *J. Am. Chem. Soc.* **124**, 2568-2583 (2002).
10. Eddaoudi, M., Kim, J., Vodak, D., Sudik, A., Wachter, J., O'Keeffe, M. & Yaghi, O. M. *Proc. Natl. Acad. Sci. U.S.A.* **99**, 4900-4904 (2002).
11. Heintz, R. A., Zhao, H., Ouyang, X., Grandinetti, G., Cowen, J. & Dunbar, K. R. *Inorg. Chem.* **38**, 144-156 (1999).
12. Biradha, K., Hongo, Y. & Fujita, M. *Angew. Chem. Int. Ed.* **39**, 3843-3845 (2000).
13. Grosshans, P., Jouaiti, A., Hosseini, M. W. & Kyritsakas, N. *New J. Chem, (Nouv. J. Chim,)* **27**, 793-797 (2003).
14. Takeda, N., Umemoto, K., Yamaguchi, K. & Fujita, M. *Nature (London)* **398**, 794-796 (1999).
15. Eddaoudi, M., Kim, J., Rosi, N., Vodak, D., Wachter, J., O'Keeffe, M. & Yaghi, O. M. *Science* **295**, 469-472 (2002).
16. Kesanli, B., Cui, Y., Smith, M. R., Bittner, E. W., Bockrath, B. C. & Lin, W. *Angew. Chem. Int. Ed.* **44,** 72-75 (2005).
17. Cotton, F. A., Lin, C. & Murillo, C. A. *Inorg. Chem.* **40**, 478-484 (2001).

MOF-2 (Monoclinic)

Experimental and Refinement Details for MOF-2:

A colorless plate type crystal (0.36 × 0.24 × 0.12 mm^3) of MOF-2 was mounted on 0.7 mm diameter nylon CryoLoops (Hampton Research) with Paraton-N (Hampton Research). The loop was mounted on a *SMART APEX* three circle diffractometer equipped with a CCD area detector (Bruker Systems Inc., 1999a)[19] and operated at 1500 W power (50 kV, 30 mA) to generate Mo K_α radiation (λ=0.71073 Å). The incident X-ray beam was focused and monochromated using Bruker Excalibur Gobel mirror optics. A total of 13948 reflections were collected of which 8717 were unique and 2476 of these were greater than 2σ (*I*). The range of θ was from 2.96 to 29.10º. Analysis of the data showed negligible decay during collection. The structure was solved in the monoclinic $P2_1/c$ space group, with Z = 21, using direct methods. All the atoms were refined anisotropically with hydrogen atoms generated as spheres riding the coordinates of their parent atoms. Modeling of electron density within the voids of the frameworks did not lead to identification of solvent molecules in all structures due to the lowered resolution of the data. The attempts made to model the solvent molecules did not lead to identification it in all structures due to the limited periodicity of the solvent molecules in the crystals. Since the solvent is free in the framework this can be expected for the MOF structures. However, very high displacement parameters, high esd's and partial occupancy due to the disorder make it impossible to determine accurate positions for these solvent molecules. Thus, electron density within void spaces which could not be assigned to any definite guest entity was modeled as isolated carbon and oxygen atoms, and the foremost errors in all the models lies with assignment of guest electron density. To prove the correctness of the atomic positions in the framework the application of the

SQUEEZE routine of A. Spek has been performed. The unit cell of MOF-2 contains 2 units of ANIC and per cadmium ion. Final full matrix least-squares refinement on $F2$ converged to R_1 = 0.1121 ($F > 2\sigma F$)) and wR_2 = 0.3653 (all data) with GOF = 1.468. It should be noted that other supporting characterization data (*vide infra* Section S1) are consistent with the crystal structure.

Table S1. Crystal data and structure refinement for MOF-2:

Empirical formula	C48 H55 N4 O19 Zn3
Formula weight	1188.13
Temperature	298(2) K
Wavelength	0.71073
Crystal system	Monoclinic
Space group	*P 21/c*
Unit cell dimensions	*a* = 33.348(3) Å α = 90° *b* = 9.8022(8) Å β = 92.442(5) ° *c* = 18.1291(8) Å γ = 90°
Volume	5920.7(7)
Z	21
Density (calculated)	1.340
Absorption coefficient	1.275
F(000)	2476
Crystal size	0.36 × 0.24 × 0.12 mm^3
Theta range for data collection	2.96 – 29.10
Index ranges	-35= h <= 44,-12<= k <= 12,-24<= l <= 24
Reflections collected	13948
Independent reflections	8717
Completeness to theta = 26.02°	85.2 %
Absorption correction	Semi-empirical from equivalents
Refinement method	Full-matrix least-squares on F^2
Data / restraints / parameters	13948 /0/560
Goodness-of-fit on F^2	1.468
Final R indices [I>2sigma(I)]	R_1 = 0.1121, wR_2 = 0.3653
R indices (all data)	R_1 = 0.1524, wR_2 = 0.3982
Largest diff. peak and hole	0.277 and – -2.745 e$Å^{-3}$

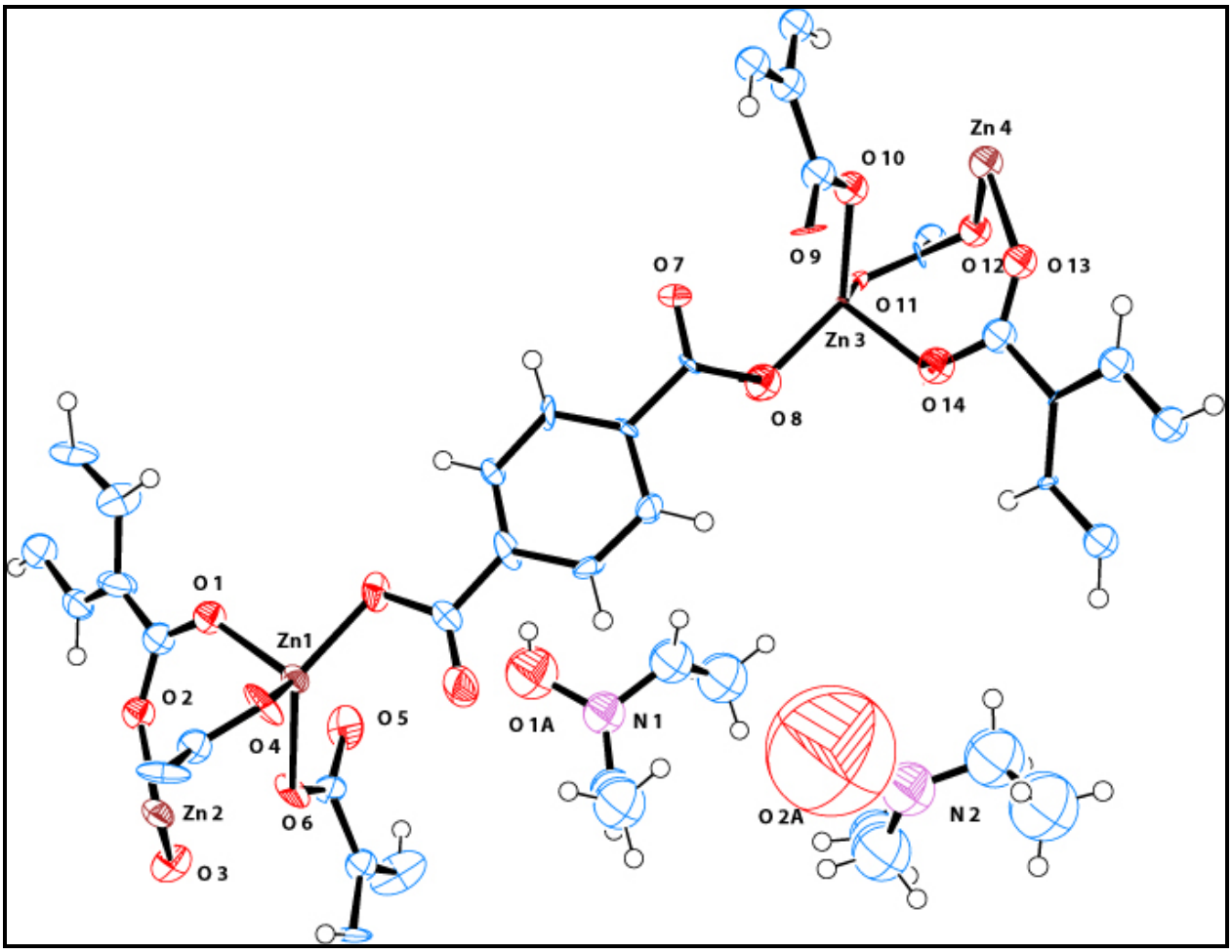

Figure S4. *ORTEP drawing of the asymmetric unit of MOF-2.*

Section 4: High Resolution Transmission Electron Microscopy (HRTEM):

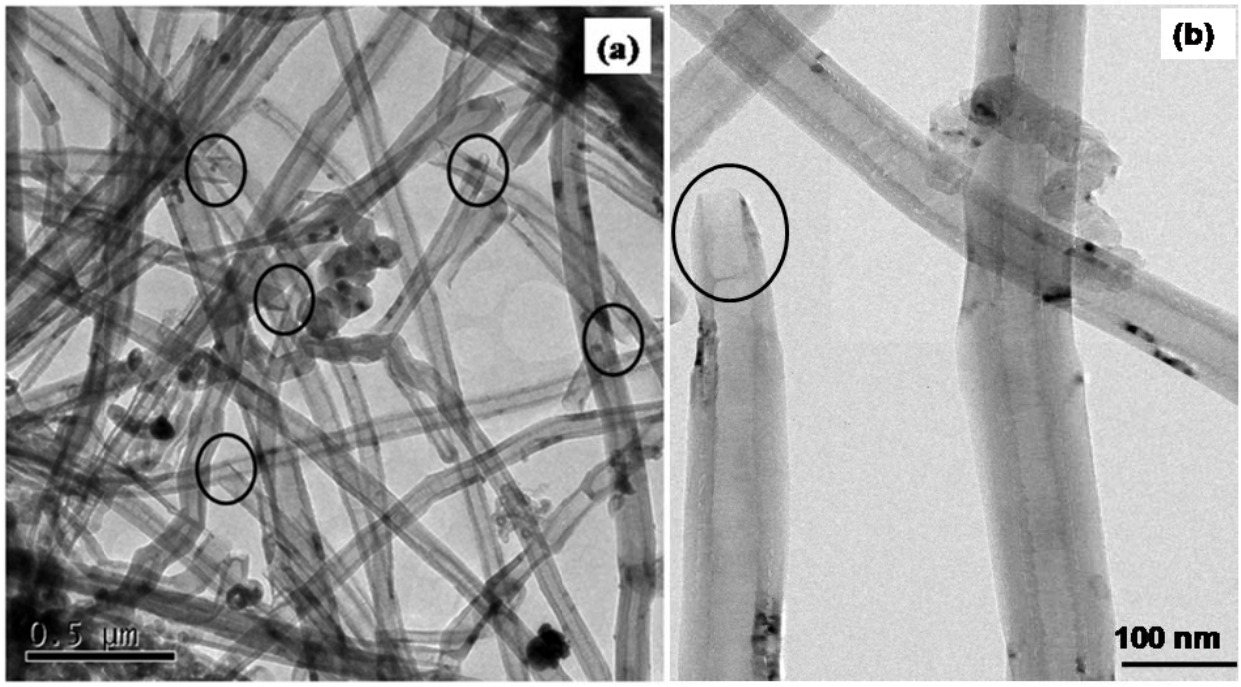

Figure S5: *HRTEM images of pristine CNF at different magnifications, (a) pristine carbon nanofiber [CNF]; encircled regions represent the open tips of the carbon nanofiber support, (b) images of carbon nanofiber clearly depicting the active terminal graphene edges and the deactivated outer wall due to the deposition of a pyrolytic carbon layer.*

Figure S4 shows the HR-TEM images of carbon nanofiber support. It is clear from Figure S4 (a) that these nanofibers are having large central hollow core and open tips. The open tips are encircled in Figure S4 (a) and (b). Figure 1(b), which is the enlarged view of carbon nanofiber clearly depicts that unlike carbon nanotubes, which are made by the simple rolling of graphene sheets, this material is made up of truncated conical graphene layers. Because of this peculiar rolling of graphene sheets, carbon nanofiber exhibits a large central hollow core, which in turn imposes a significant portion of exposed and reactive edges in the inner channel created within the carbon nanofibers as highlighted in the blue box. However, the edge sites on the outer surface of the nanofibers are clearly covered by the deposition of a pyrolitic carbon layer induced

by the high reaction temperature in the synthesis of this material. This peculiar morphology of the material leaves its inner wall inherently active and outer wall inert. At the same time, the relatively large inner diameter, open tips, active inner wall and possibility of activating the inert outer wall by facile chemical treatments make this a potential support material for effectively dispersing various materials on both the outer walls and in the inner cavity.

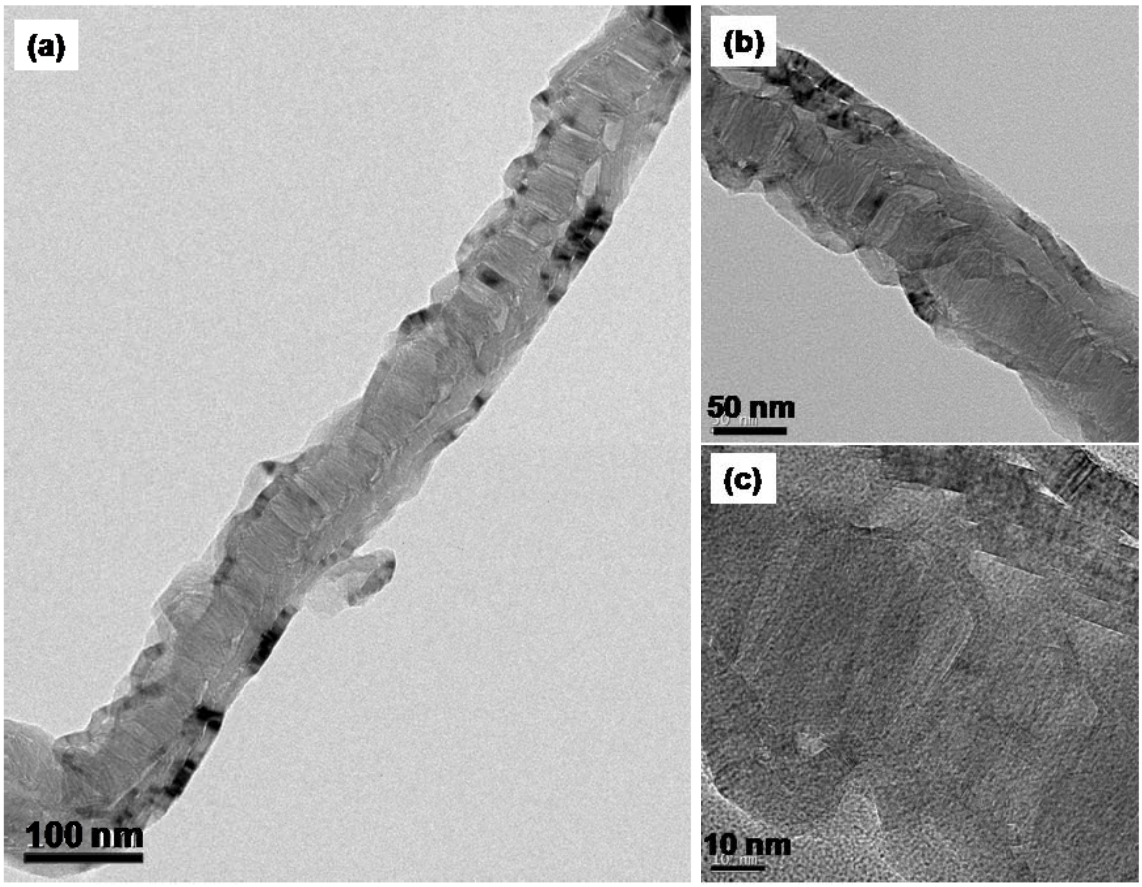

Figure S6: *(a) and (b) HRTEM images of MOF@PCNF at different magnifications are clearly showing the one-dimensional confinement of nanosized MOFs in the inner cavity of CNFs. (c) image showing the continuous lattice fringes clearly indicating the crystalline nature of the MOFs.*

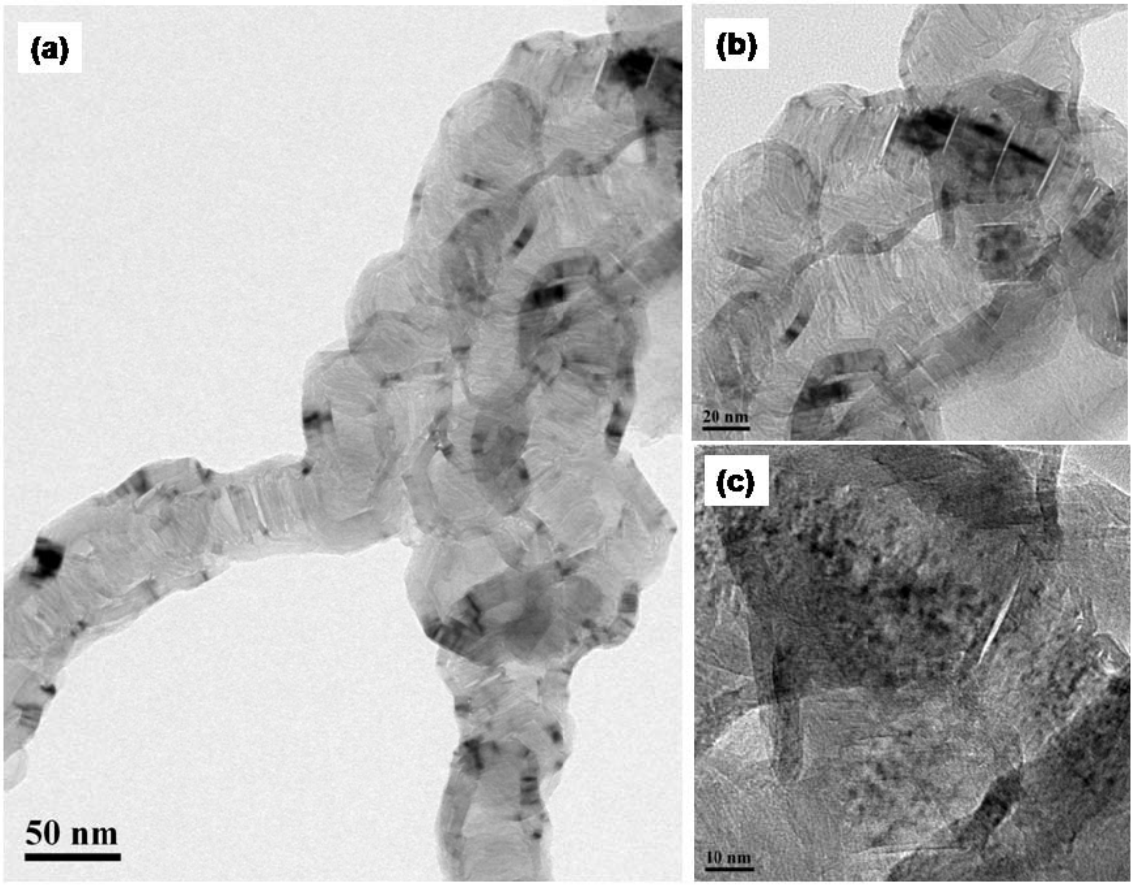

Figure S7 A: *(a) and (b) HRTEM images of MOF@FCNF at different magnifications are depicting the attachment of MOFs on the outer walls along with its confinement in the inner cavity. (c) image showing the continuous lattice fringes clearly indicating the crystalline nature of the MOFs both in the inner cavity as well as on the outer walls.*

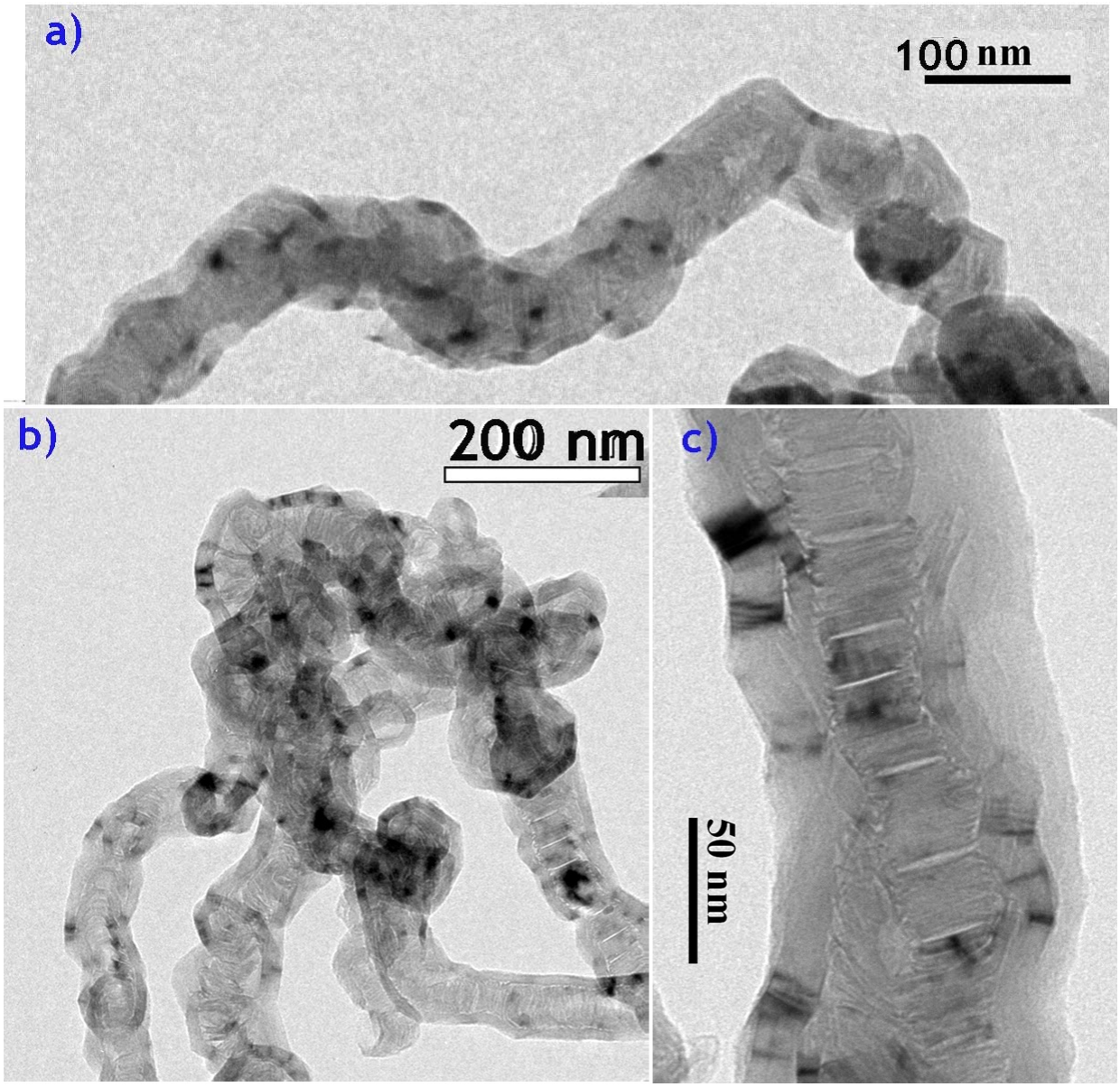

Figure S7 B: *HRTEM images of MOF@FCNF at different magnifications are depicting the attachment of MOFs on the outer walls along with its confinement in the inner cavity.*

Section 5: X-ray Photoelectron Spectroscopy (XPS):

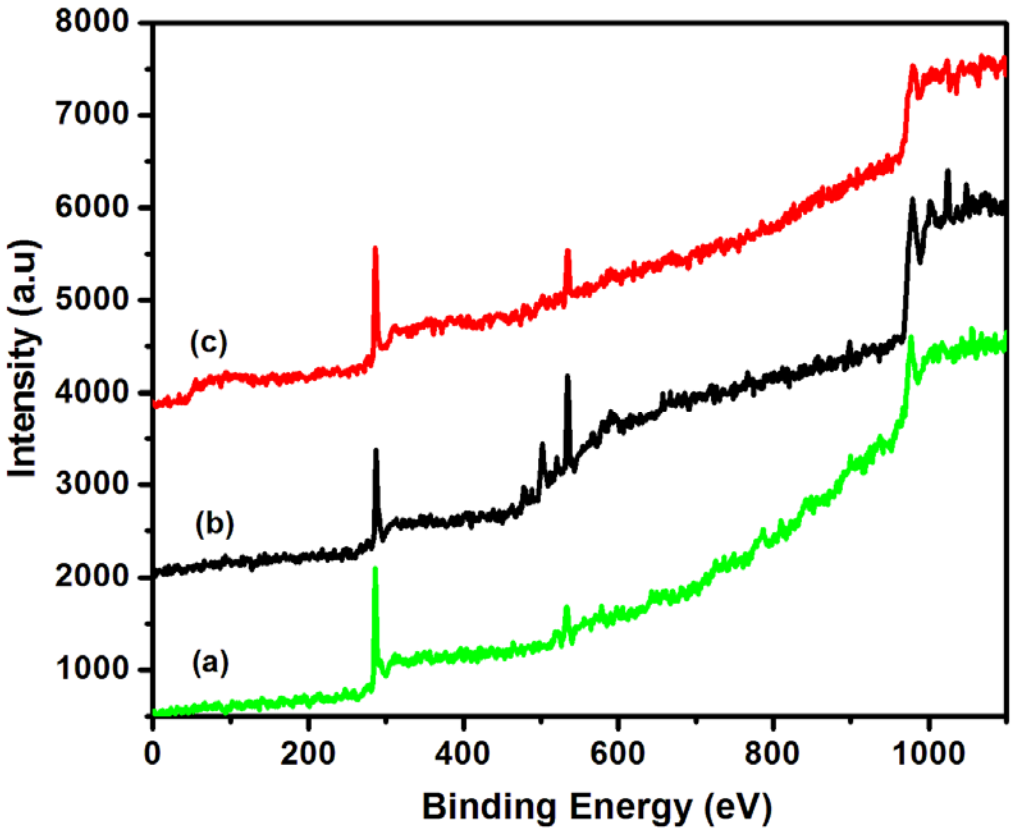

Figure S8: *Comparison of the full survey X-ray photoelectron spectra obtained for (a) FCNF, (b) MOF-2 and (c) MOF@FCNF.*

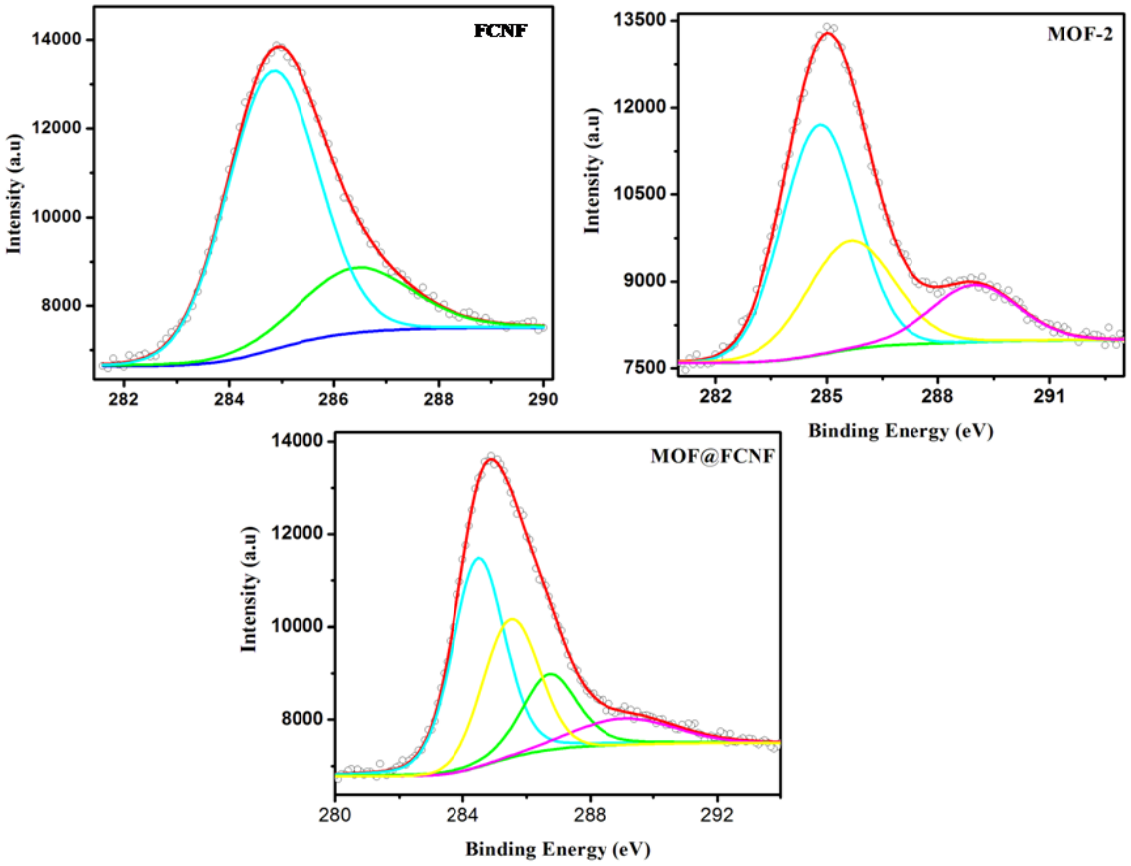

Figure S9: *XP spectra of C 1s core level of F-CNF, MOF-2 and MOF@FCNFs after deconvolution; the circles represent the experimental data, red line represents the fitting data for the overall signal and the dotted lines are the deconvoluted individual peaks for different species present in the sample.*

The comparison of the C1s part of FCNF, MOF-2 and MOF@FCNF is given in Figure S6. The C part of FCNF after deconvolution gives the hydrocarbon C 1s peak at 285 eV and the peak corresponding to the carbon attached to hydroxyl functional groups at 286.4 eV. Pure MOF2 show three peaks at 284.8, 288.9 and 285.6 eV respectively in the carbon region which can be assigned to the hydrocarbon C1s and the carbon coordinated to one Zn^{+2} and two Zn^{+2} through the oxygen atoms. The carbon spectra of MOF-2@CNFs give one additional peak at binding energy 286.7 eV after deconvolution which can be assigned to the F-CNF carbon attached to Zn^{+2} of the MOF-2 through the oxygen containing functional groups.

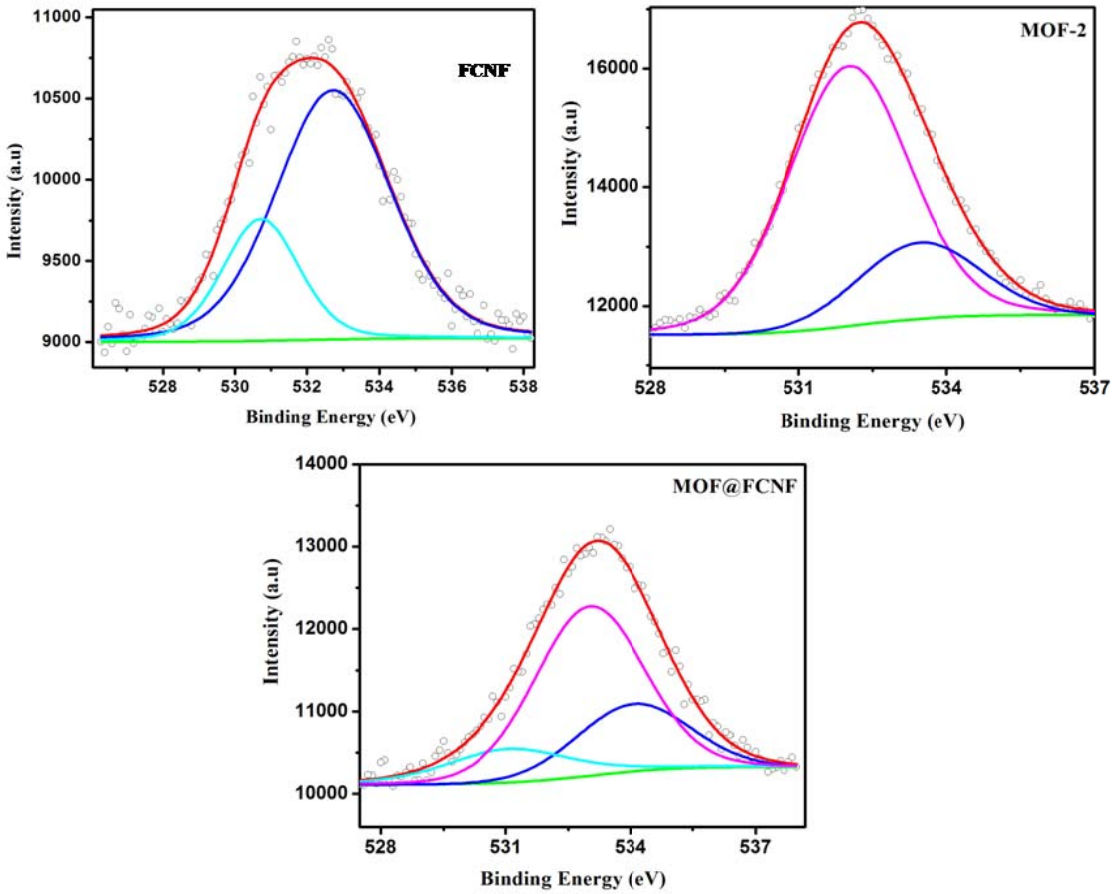

Figure S10: *Comparison of XP spectra of O 1s core level of F-CNF, MOF-2 and MOF@FCNFs after deconvolution; the circles represent the experimental data, red line represents the fitting data for the overall signal and the dotted lines are the deconvoluted individual peaks for different species present in the sample.*

The efficient incorporation and the existence of the interaction are supplemented by the comparison of the O 1s spectra of FCNF, MOF-2 and the hybrid MOF@CNFs also [Figure S7]. FCNF shows two peaks in the O spectrum at 530.7 and 532.7 eV which can be assigned to the oxygen present in the functional groups and the traces of oxide impurity present in the sample respectively. Pure MOF-2 gives two peaks at 532 and 533.5 eV which are respective to the oxygen in the ZnO4 moiety and the free oxygen in the crystal which confirms the formation of MOF. In exact agreement with the C1s and Zn 2p spectra of the MOF@FCNFs, the oxygen part

also exhibited one additional peak at 531.7 eV which is probably due to the oxygen of the FCNF attached to Zn^{+2} in the MOF-2.

Section 6. TGA data and the thermal stability of MOF and MOF@FCNF:

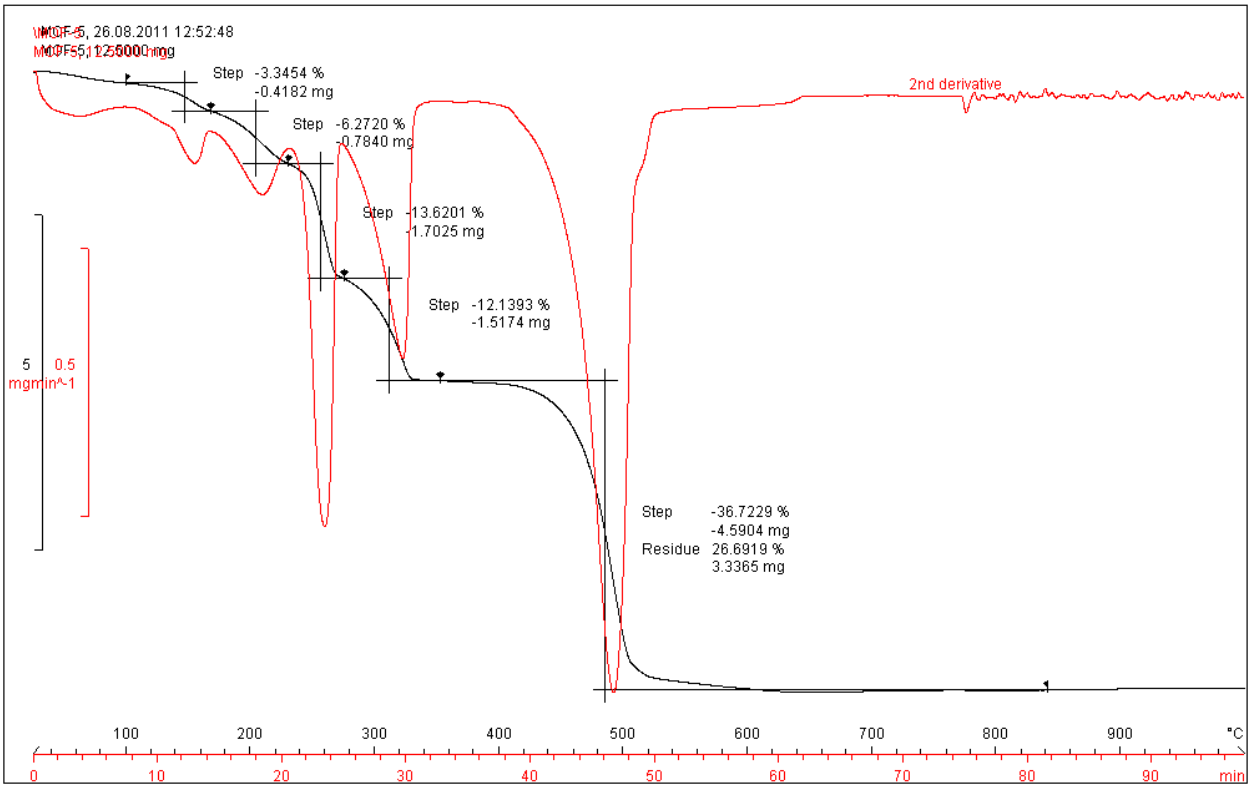

Figure S11. *Thermal stability and the thermal gravimetric analysis (TGA) data of MOF-2.*

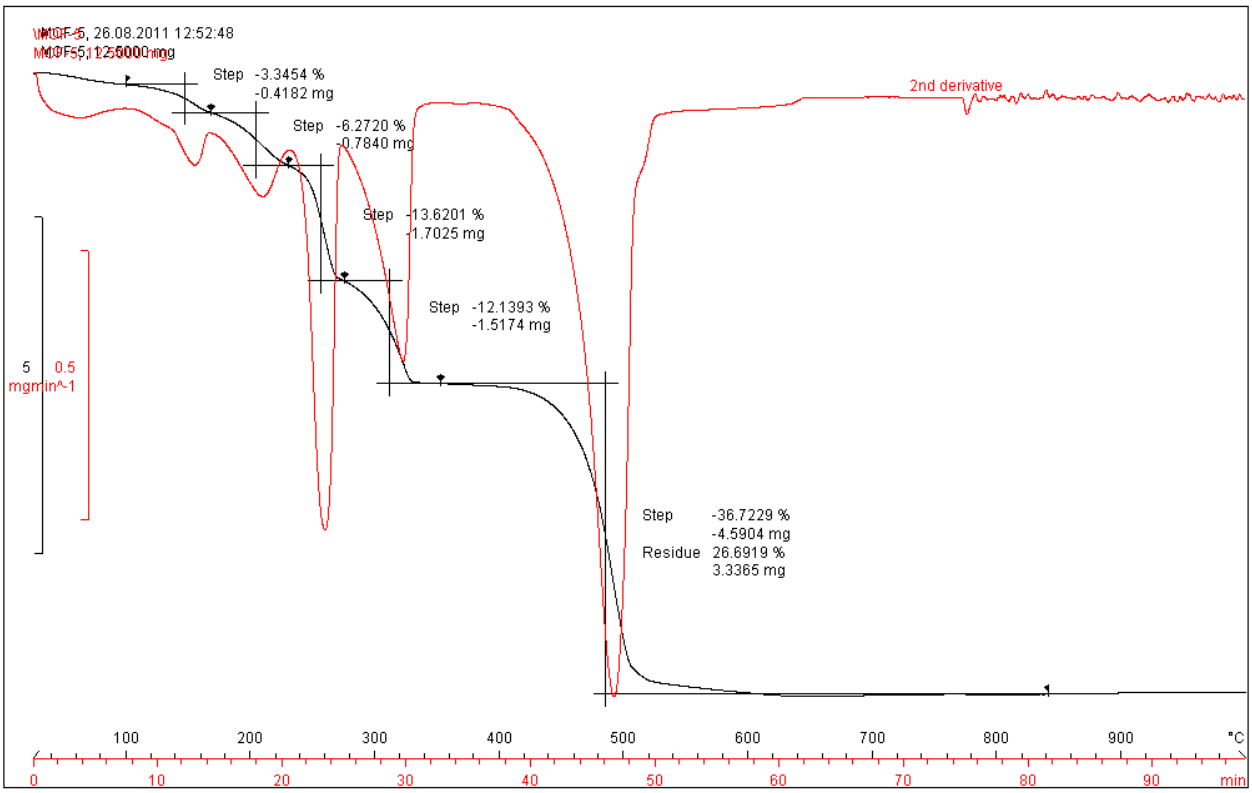

Figure S12. *Thermal stability and the thermal gravimetric analysis (TGA) data of MOF@FCNF.*

Section 7. IR data of FCNF, MOF-2 and MOF@FCNF:

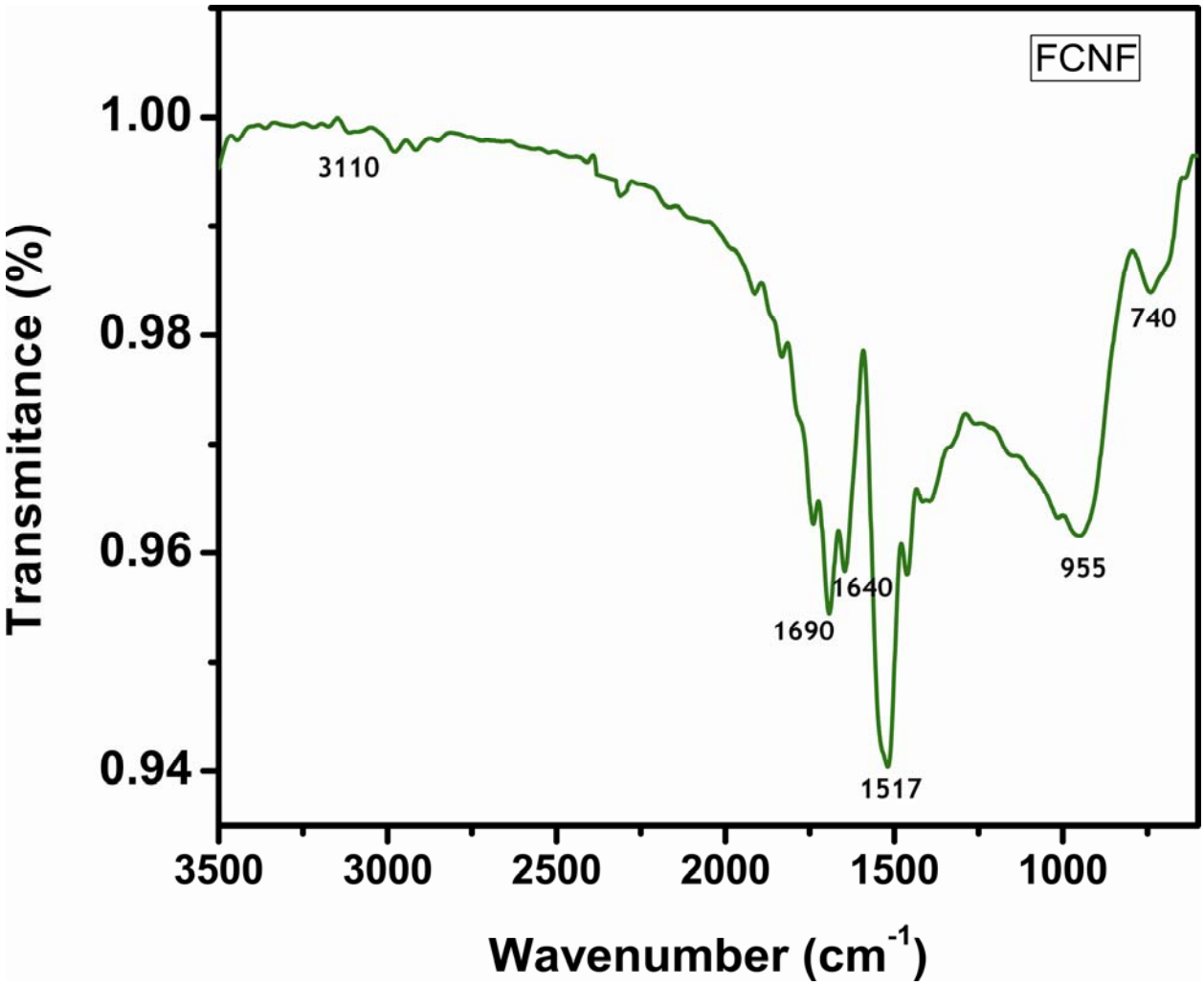

Figure S13. *IR spectra of Functionalized CNF.*

3110 cm^{-1}: O-H functional group stretching.

1690 cm^{-1}: C-O stretching.

1640 cm^{-1}: C=C sp^2 bonds

1517 cm^{-1}: Aromatic C=C

955 cm^{-1}: Substituted alkenes

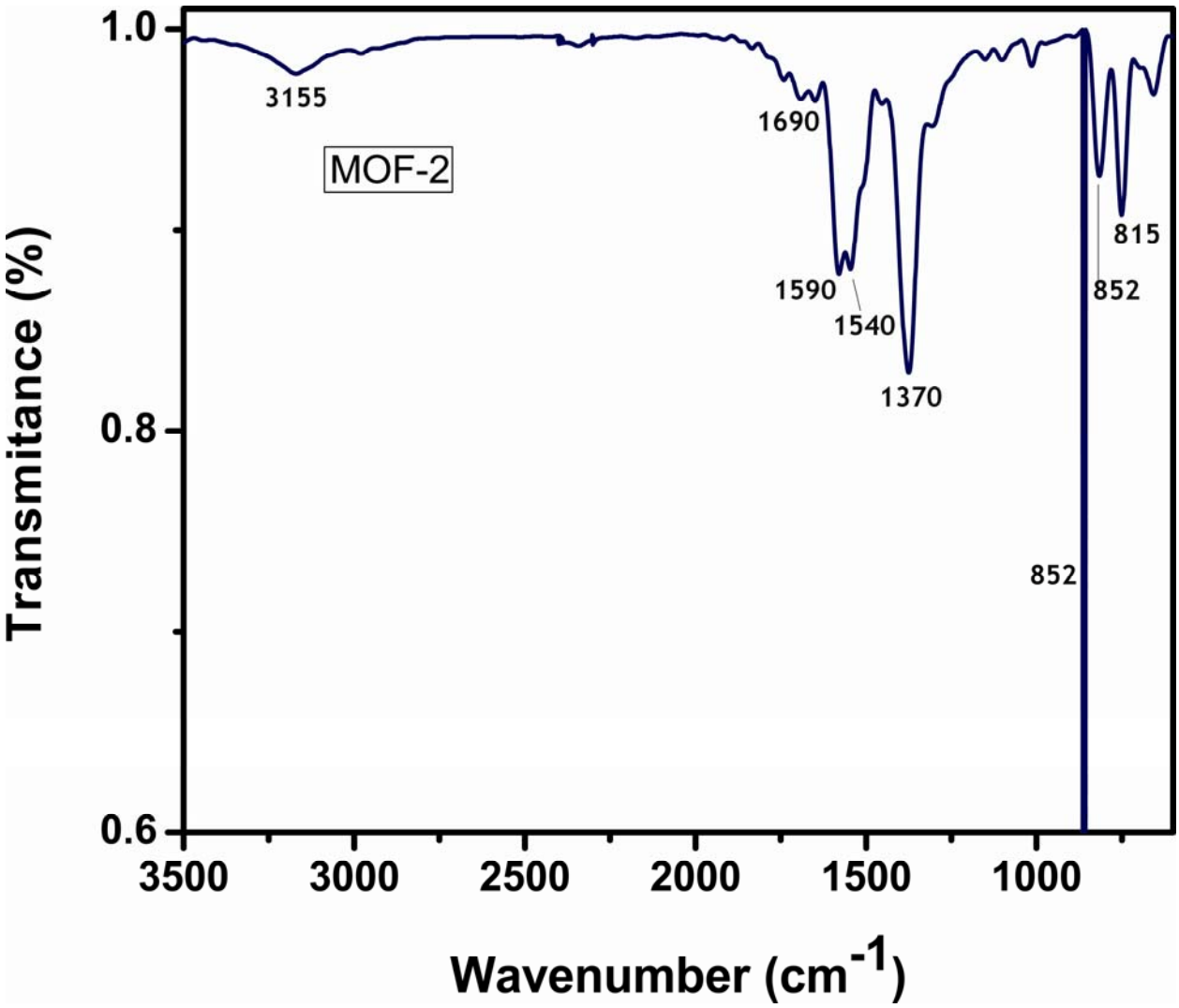

Figure S14. *IR spectra of pure MOF-2.*

3155 cm^{-1}: O-H functional group stretching.

1690 cm^{-1}: C-O stretching.

1590 cm^{-1}: C=C sp^2 bonds

1540cm^{-1}: Aromatic C=C

1370 cm^{-1}: C≡C-H (bending)

890 cm^{-1}: $C=CH_2$

815 cm^{-1}: Para di-substituted Benzene

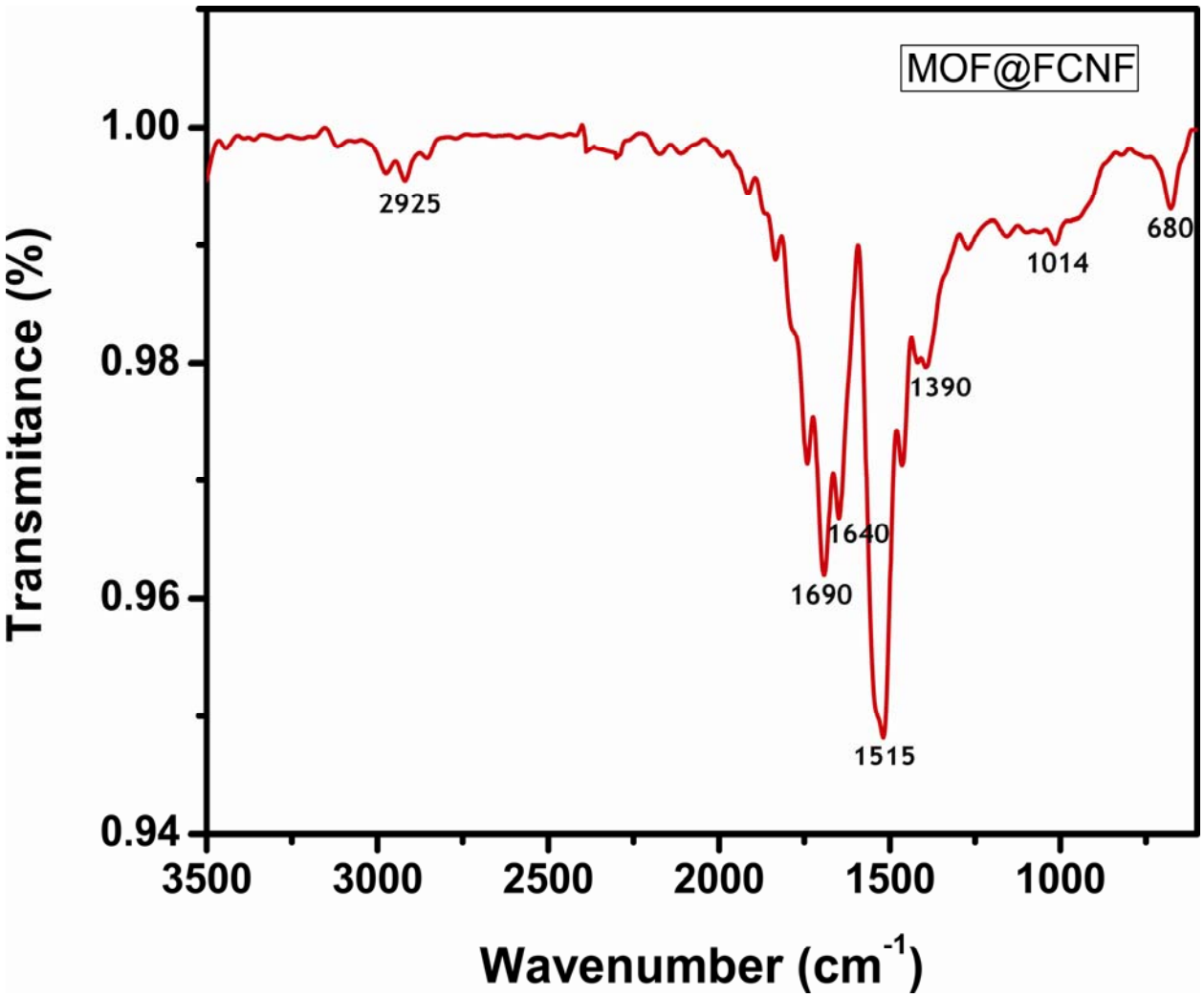

Figure S15. *IR spectra of MOF-2@FCNF hybrid.*

2925 cm^{-1}: C–H stretch.

1690 cm^{-1}: C-O/Zn-O stretching.

1640 cm^{-1}: –C=C– stretch

1515 cm^{-1}: C–C stretch (in–ring)

1390cm^{-1}: C–H rock

1014 cm^{-1}: =C–H bending

Section 8. Gas adsorption analysis and N_2 adsorption isotherms for MOF@FCNF, MOF-2 and FCNF:

Since CNF is a hollow structure with a large central hollow core and comparatively larger inner diameter (60 ± 10 nm), diffusion of guest molecules into the inner cavity will not be a major problem. But on the other hand, adsorption of tiny gas molecules like N_2 (Kinetic diameter-3.65 Å), CO_2 (Kinetic diameter-3.4 Å) and H_2 (Kinetic diameter-2.85 Å) is also difficult in case of CNFs, as they have very high diameter compared to the kinetic diameter of the adsorbing molecules. Form the synthesis part; it is clear that relatively viscous N, N- Diethylformamide (DEF) solution has entered in the inner cavity without any diffusional limitation resulting into the formation of MOF-2 crystals in the inner cavity. Since in the case of gas uptake, the molecules are in the gaseous state, so diffusional limitation will be less as compared to that in the liquid phase. Moreover, the CNF is not completely packed with the MOFs thus leaving path for gas diffusion. During the mass-transport process, the guest molecules can either diffuse through the pore (Knudson diffusion or bulk diffusion), on the pore wall (surface diffusion) or a combination through desorption/adsorption processes. In this context, although CNFs are partially or completely filled with the MOF-2, the active graphene edges which are still present inside the CNFs, which acts as adsorption sites. As MOF-2 itself is porous, it can easily adsorb or allow the diffusion of gas molecules through its pores and through the CNFs. MOF@CNF although have limited channels, the overall increase in the gas uptake can be attributed to the creation of the new adsorption sites (active graphene edges) as well synergetic effect of both MOF as well as CNFs. But we would like to mention that the exact mechanism of the adsorption of gases on the MOF@CNF is still not clear, we are still finding the ways to analyze the reason behind the overall increase in the gas uptake rather than FCNF and MOF-2.

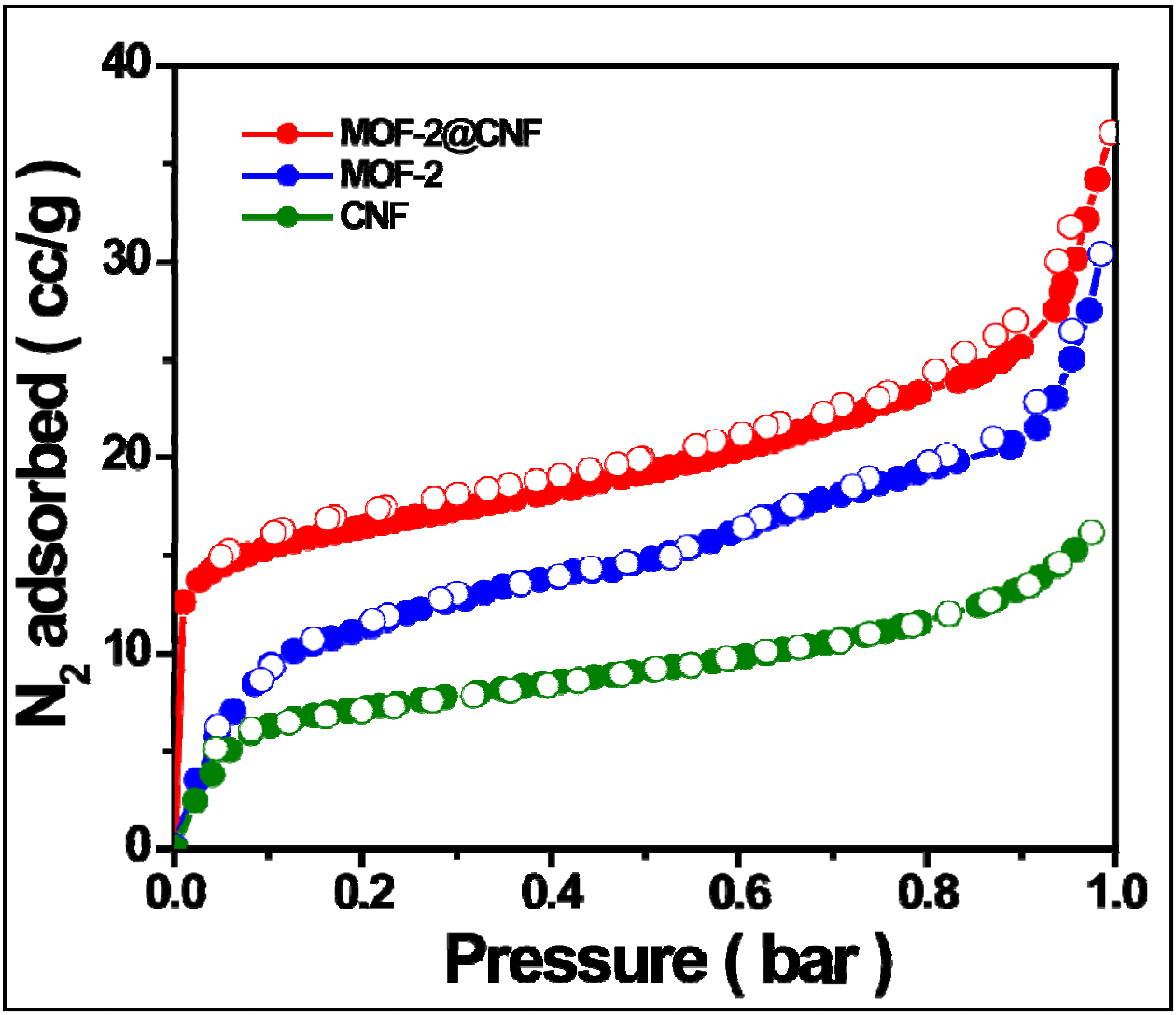

Figure S16. *Typical Type-I nitrogen adsorption isotherms for MOF-2@FCNF, MOF-2 and FCNF at 77 K and 1 atm pressure.*

Section 9. Single crystal structures of MOF-2:

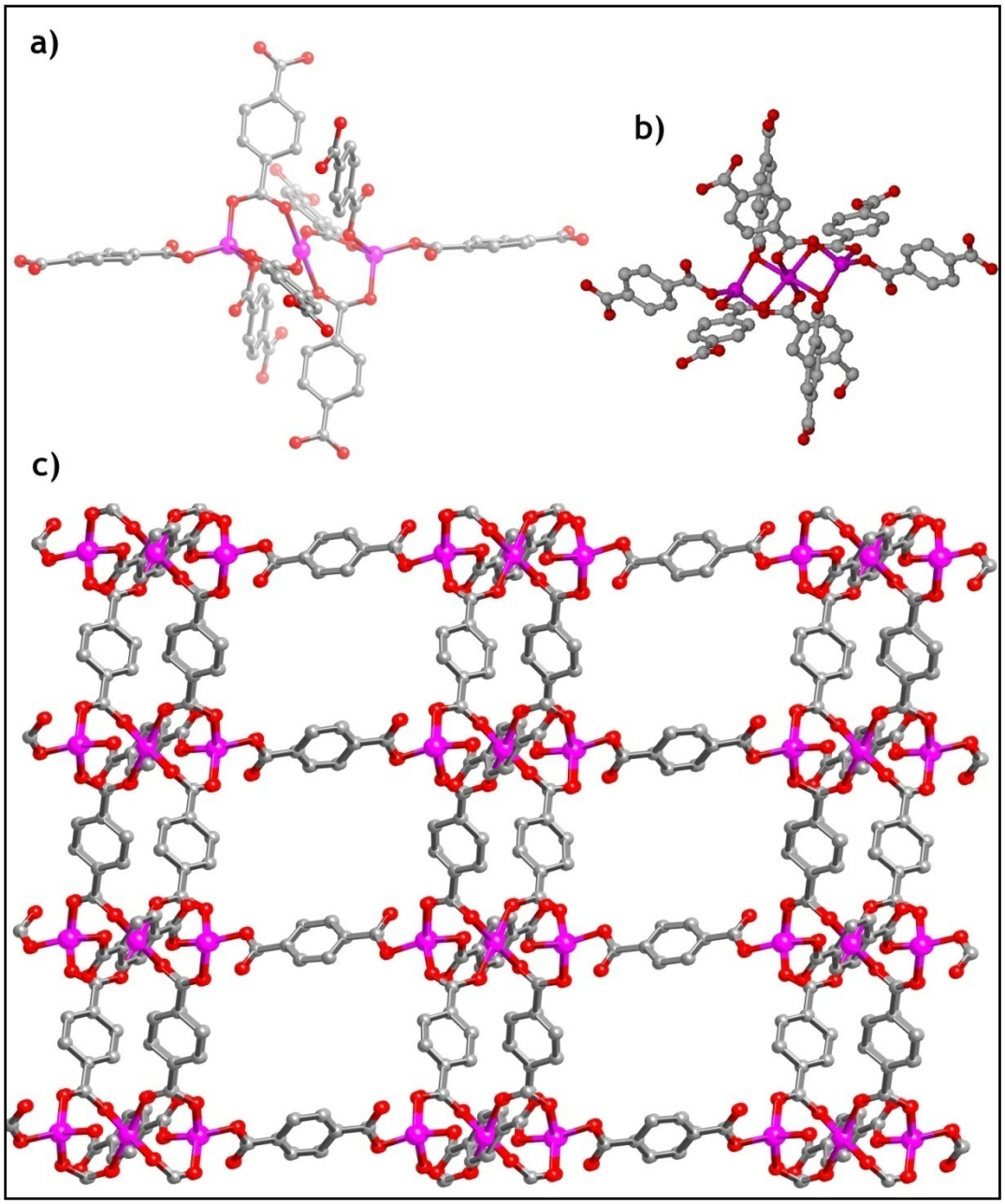

Figure S17. *Crystal structure of MOF-2. (a) Tetrahedral SBU's in MOF-2 where each tetrahedral Zn is connected to the next Zn through bridging carboxylate groups. (b) Octahedral SBU in MOF-2, sandwiched between 2 tetrahedral Zn atoms. c) Packing diagram of MOF-2 through b axis showing one dimensional channels running through structure. Hydrogen atoms and guest molecules are omitted for clarity. Color code: Zn (Pink), O (red), C (gray).*

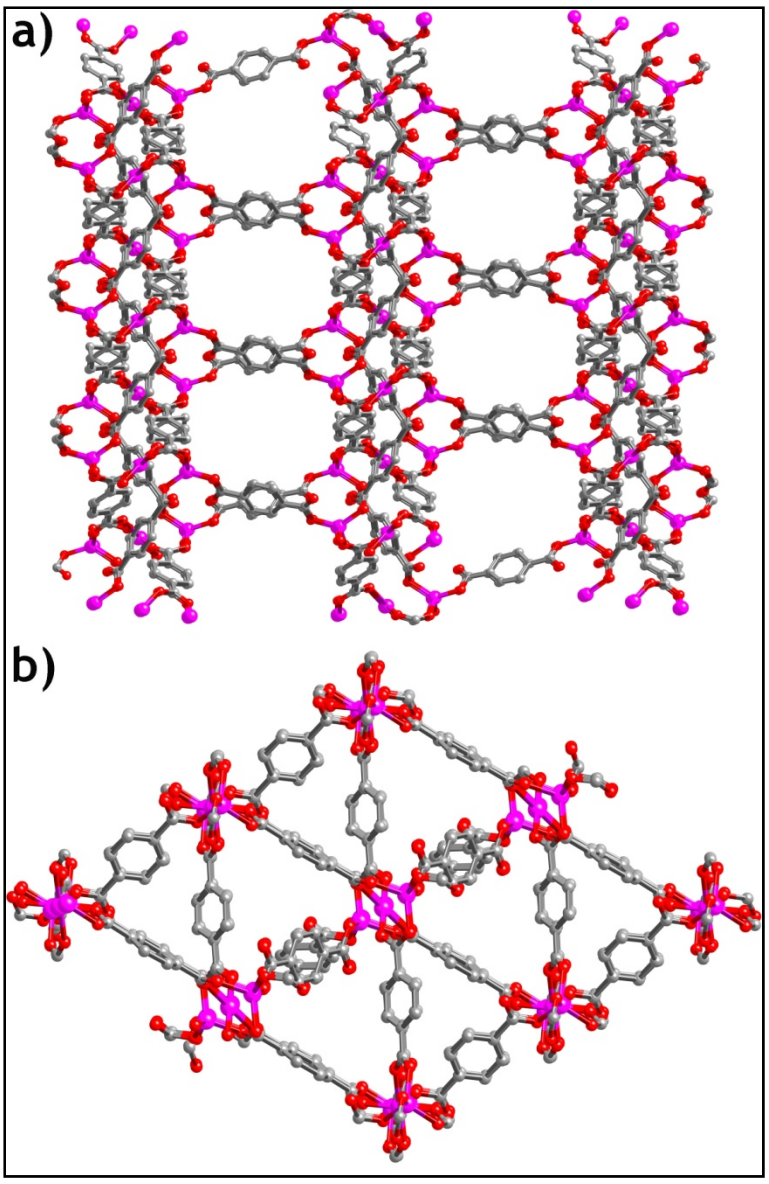

Figure S18. *Crystal structure of MOF-2. (a) Packing diagram of MOF-2 through c axis showing one dimensional channels running through structure. b) Packing diagram of MOF-2 showing Zn and terephthalic acid connectivity. Hydrogen atoms and guest molecules are omitted for clarity. Color code: Zn (Pink), O (red), C (gray).*